

Introducing γ -lifting for Learning Nonlinear Pulse Shaping in Coherent Optical Communication

Tim Uhlemann, Alexander Span, Sebastian Dörner, and Stephan ten Brink

Institute of Telecommunications

University of Stuttgart

Pfaffenwaldring 47, 70569 Stuttgart, Germany

{uhlemann,span,doerner,tenbrink}@inue.uni-stuttgart.de

Abstract—Pulse shaping for coherent optical fiber communication has been an active area of research for the past decade. Most of the early schemes are based on classic Nyquist pulse shaping that was originally intended for linear channels. The best known classic scheme, the *split digital back propagation*, uses joint predistortion and post-equalization and hence, a *nonlinear* transmitter; it, however, suffers from spectral broadening on the fiber due to the Kerr-effect. With the advent of deep learning in communications, it has been realized that an “autoencoder” can learn to communicate efficiently over the optical fiber channel, jointly optimizing geometric constellations and pulse shaping – while also taking into account linear and nonlinear impairments such as chromatic dispersion and Kerr-nonlinearity. E.g., [1] shows how an autoencoder can learn to mitigate spectral broadening due to the Kerr-effect using a trainable *linear* transmitter. In this paper, we extend this *linear* architectural template to a scalable *nonlinear pulse shaping* consisting of a convolutional neural network at both transmitter and receiver. By introducing a novel γ -lifting training procedure tailored to the nonlinear optical fiber channel, we achieve stable autoencoder convergence to pulse shapes reaching information rates outperforming the classic split digital back propagation reference at high input powers.

Index Terms—autoencoder, communication, optical, coherent, nonlinear, chromatic dispersion

1. Introduction

For the design of an optical fiber communication system that achieves a high spectral efficiency (SE) one requires higher order modulation formats and thus a high signal-to-noise-ratio (SNR) at the receiver (RX). This, in turn, needs higher launch powers at the transmitter (TX). Furthermore, a time-bandwidth-product (TBP) close to one should be chosen to not limit the SE, i.e., symbol rate and occupied bandwidth should almost equal. This, in general, holds for the copper and wireless (radio frequency) channel. In contrast, for the optical fiber, a high input power results in a large Kerr-nonlinearity and hence, in a highly distorted signal at the RX [2]. Apart from the signal-noise interaction, in a single channel scenario, this nonlinearity-induced distortion is deterministic and may be mitigated at TX or RX. Nevertheless, to obtain an optimal equalization performance, one is either forced to take into account the Kerr-nonlinearity-induced spectral

broadening and, thus, support a wider bandwidth compared to the chosen symbol rate [3], [4]; or, operate in a regime where spectral broadening can be neglected [5]. The first approach reduces SE, whereas the second limits design and hardware options; For instance regarding the symbol rate, as spectral broadening inversely increases with it (as will be shown later).

Our superimposed goal is to develop a communication system that is able to overcome the need for additional bandwidth but still achieves optimal (or at least a better) performance than conventional reference systems.

For those, digital signal processing (DSP) algorithms have shown to outperform physical methods such as optical phase conjugation [6], or optical back propagation [7]. Digital approaches can be further divided into three types, (i) a static, analytical, and conventional equalization by fixed algorithms, such as the Volterra-series [8], digital back propagation (DBP) [9], and perturbation models [10]; (ii) nonlinear Fourier transform (NFT)-based schemes [11]; or (iii) deep-learning (DL) techniques with architectural templates based on the aforementioned conventional systems – or based on, e.g., a neural network (NN) [12].

As will be shown later, the DBP is able to compensate for channel impairments almost perfectly up to a certain launch power where signal-noise interaction becomes relevant. This is already known and expected as it is the ideal inverse of the split-step Fourier method (SSFM)-algorithm used to simulate the optical channel. Nevertheless, by limiting the bandwidth of TX and RX the performance decreases significantly due to spectral broadening only. This way we can show that the later introduced autoencoder (AE) is able to compensate for spectral broadening and, hence, allows to operate at higher input powers when compared to conventional systems. One particularity is that training the proposed structure requires a specific procedure that we refer to as “ γ -lifting” to achieve stable convergence, and to find better local optima.

This paper, thereby, reports significant progress over [1], where an AE with linear TX was trained to mitigate spectral broadening at high input powers. The training results there have shown that the AE is still not fully able to compensate for the aforementioned nonlinear impairments at higher input powers $P > 5$ dBm. Hence, here, we extend the AE of [1] to include a nonlinearity compensation (NLC) architecture, effectively implementing a nonlinear TX. Note that the linear TX of [1] is still contained within the new model as a special case, allowing simple evaluation of the additional gains. The

arXiv:2207.06089v1 [cs.IT] 13 Jul 2022

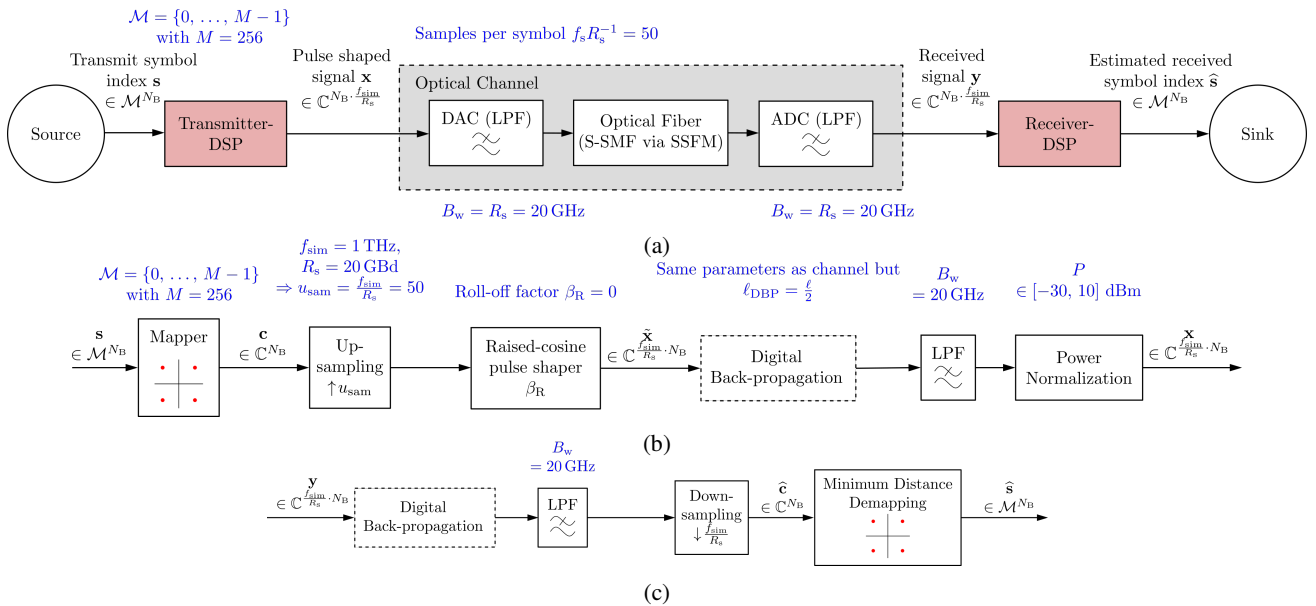


Figure 1: System model with (a) overview that holds for conventional as well as AE setup, (b) the DSP for the conventional TX, and (c) the RX based on split DBP.

nonlinear extension is thereby inspired by the split DBP consisting of a nonlinear and joint mitigation at TX and RX, currently providing the best performance [13].

DL-techniques are already widely used in almost all parts of an optical communication system. The novelty of this paper is the application of an architectural template with nonlinear TX, i.e., its pulse shaping, as well as its particular training method. In a similar spirit, e.g., Häger et al. [14], proposed a trainable SSFM, or DBP, at the RX of which the first half of the compensating path may be moved to the TX and used as predistortion (PD). Despite the fact that our trainable architectural template is not based on the SSFM, we train the PD directly as part of the TX. This allows the TX to learn the opportunities of a PD seeing all subsequent components. Neskorniuk et al. [15] have used a trainable nonlinear PD based on cubic correction terms over an approximated channel model applying the perturbation method. There, they have shown that the training can be significantly stabilized and accelerated up to a specific input power. However, we operate at input powers where this alternative channel model differs too much from the more accurate SSFM, which we have applied in this work. Further, we also included the quasi-analog pulse shaping into the training. Gaiarin et al. [16] have trained a transmitter based on the NFT [17], providing another nonlinear TX structure. Yet, it has been shown that NFT-based systems are currently far from spectrally efficient operations [16].

The remainder of this work is structured as follows. Section 2 provides a short description of the channel, the considered DBP, as well as its performance drop at high launch powers. In section 3 the architectural template of the AE is introduced including the nonlinear TX. Section 4 proposes a new training procedure tailored to the optical fiber channel that leads to improved equalization capabilities of the AE. Finally, section 5 renders some conclusions and provides an outlook to future extensions.

2. System model and performance references

The channel model used in this work is taken from [1] comprising the band-limited digital to analog converter (DAC) (represented by a lowpass filter (LPF)), the optical fiber, and a band-limited analog to digital converter (ADC), i.e., again an LPF as shown in the dashed gray box of Fig. 1a. All LPFs are ideally rectangular shaped. This model not only holds for the reference system but also for the AE as introduced later.

The optical fiber is simulated via the symmetric SSFM following the Wiener-Hammerstein model and, thus, approximating a solution of the nonlinear Schrödinger equation (NLSE) [18]

$$\frac{\partial q(t, z)}{\partial z} = j \frac{\beta_2}{2} \frac{\partial^2 q(t, z)}{\partial t^2} - j \gamma |q(t, z)|^2 q(t, z) + n(t, z), \quad (1)$$

where ideal Raman amplification is assumed and the term accounting for fiber attenuation α was removed. Here $q(t, z)$ is the optical baseband signal with time t and distance z . Alongside mitigating the attenuation, the amplification introduces noise $n(t, z)$ with power spectral density

$$\rho_n = n_{\text{sp}} h f_0 \alpha. \quad (2)$$

The corresponding channel parameters are summarized in Tab. 1. As we consider a single channel and single polarization system the only observable manifestation of the Kerr-effect is self phase modulation (SPM).

Among the fiber parameters, also some of the signal processing, e.g., those of the converters or DSPs, are fixed to obtain comparable systems; e.g., the supported bandwidth of both converters is set to $B_w = 20 \text{ GHz}$. To avoid artificially limiting the SE we have chosen a symbol rate of $R_s = B_w = 20 \text{ GBd}$ and hence, a symbol duration of $T = 1/R_s = 50 \text{ ps}$. The simulation bandwidth is $f_{\text{sim}} = 1 \text{ THz}$ such that one obtains $f_{\text{sim}} R_s^{-1} = 50$ samples per symbol. The resulting TBP is

$$\Pi_{\text{TBP}} = T \cdot B_w = 1. \quad (3)$$

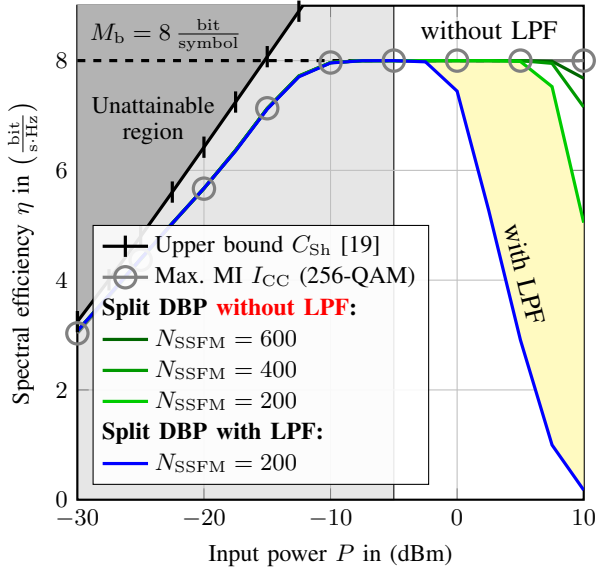


Figure 2: Comparison of the performance of a split DBP with and without (DAC/ADC-induced) LPFs.

The alphabet, or set of message symbol indices, is $\mathcal{M} = \{0, \dots, M-1\}$ with $M = 256$ and the number of transmitted symbols is N_B .

As performance measure, we use the spectral efficiency (SE) defined as

$$\eta = \frac{I(s; \hat{s})}{T \cdot B_w} = \frac{I(s; \hat{s})}{\Pi_{TB}} \stackrel{\Pi_{TB}=1}{=} I(s; \hat{s}), \quad (4)$$

where $I(s; \hat{s})$ is the mutual information (MI) between the distributions of the transmitted s and the received (hard decided) symbol indices \hat{s} as shown in Fig. 1a. Here we use histograms of hard decided symbols at RX to include the whole RX-DSP in the chosen performance measure. Obviously, the performance could be improved by using soft outputs. But, in this work, we are more interested in studying how to mitigate the drop of MI at high launch power and how to address this by means of pulse shaping.

TABLE 1: Simulation parameters.

Property	Symbol	Value
Planck's constant	h	$6.626 \cdot 10^{-34}$ J s
Carrier frequency	f_0	193.55 THz
Attenuation	α	0.046 km^{-1} $\cong 0.2 \text{ dB km}^{-1}$
Chromatic dispersion	β_2	$-21.67 \text{ ps}^2 \text{ km}^{-1}$
Kerr-nonlinearity	γ	$1.27 \text{ km}^{-1} \text{ W}^{-1}$
Spontaneous emission	n_{sp}	1
Fiber length	ℓ	1000 km
Simulation sampling rate	f_{sim}	1 THz
No. of SSFM-steps	N_{SSFM}	200
Fixed SSFM step-size	Δz_{SSFM}	5 km
Launch power	P	-30 dBm, ..., 10 dBm
Bandwidth of TX/RX	B_w	20 GHz

2.1. Spectral broadening revisited

Taking into account the considered power range for P , we obtain a dispersion length of

$$\ell_D = T^2 / |\beta_2| = 115 \text{ km} \quad (5)$$

and a nonlinear length of

$$\ell_{NL}(P) = 1/(\gamma P) \in [78, 78 \cdot 10^4] \text{ km} \quad (6)$$

such that $\ell_D < \ell_{NL}(P)$ does not hold for all input powers P [18]. This way we operate in a regime where spectral broadening cannot be neglected [20]. Further it holds that

$$\ell_{NL}(P) < \ell \forall P > -1.0 \text{ dBm}. \quad (7)$$

Consequently, the received signal's bandwidth definitely exceeds the supported system bandwidth $B_w = R_s$ for conventional communication systems (and their corresponding equalization) as there is no margin implemented between B_w and the original signal bandwidth R_s .¹ Next, we specify the goal for the AE more precisely to "Learning a high MI despite the effect of spectral broadening."

2.2. Limitations of Digital Back Propagation

As a reference system we use the "split DBP" or also called "split NLC" by [13]. The corresponding TX and RX are shown in Fig. 1b and Fig. 1c, respectively.

The TX consists of a conventional 256-quadrature-amplitude-modulation (QAM) that translates the symbol indices $\mathbf{s} \in \mathcal{M}^{N_B}$ to complex constellation symbols $\mathbf{c} \in \mathbb{C}^{N_B}$. An ideal Nyquist pulse-shaping (consisting of an upsampling to simulation frequency f_{sim} and a raised cosine pulse shaping with roll-off $\beta_R = 0$) lead to the bare transmit signal $\tilde{\mathbf{x}}$. Typically a two-fold oversampling is used, whereas we use an oversampling of $u_{sam} = f_{sim}/R_s = 50$ for a fair comparison with the later introduced trainable models that shall not learn to compensate any inaccuracy, and to exclude a numerical mismatch between channel and equalizer. It follows an NLC as PD that is realized by a DBP, which pre-compensates for a fiber length of $\ell_{DBP} = \frac{\ell}{2}$. A subsequent LPF plus power normalization generates the transmit signal \mathbf{x} . The RX starts with a DBP processing the received signal \mathbf{y} for a fiber length of again $\ell_{DBP} = \frac{\ell}{2}$ at simulation rate, which is already lowpass-filtered by the channel (see converters in Fig. 1a).² An LPF assures a correct down-sampling to symbol rate R_s for a subsequent minimum distance demapping. The DBP algorithm itself is based on the symmetric SSFM following the Wiener-Hammerstein model as shown in [2] that is also used for the channel simulation.

It was already shown that for a PD-only implementation "SPM can be eliminated, within experimental error, up to where the transmitter bandwidth limits are reached" [21]. Hence, in general the chosen PD leads to a transmit signal that perfectly pre-compensates for channel impairments but occupies more bandwidth than the supported one by the converters. The same holds for the

1. Note that a margin would artificially increase the TBP and, hence, lower the SE.

2. In the simulation the ADC belongs to the channel, but technically the channel has no lowpass-characteristic.

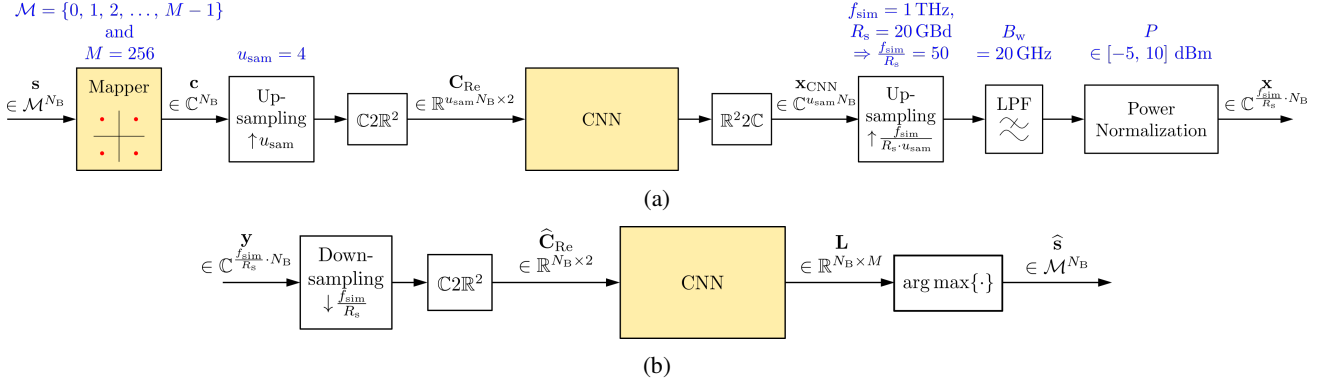


Figure 3: Architectural template of the proposed AE implementing the TX- and RX-DSP. Trainable blocks are colored in yellow. (a) shows the TX-, and (b) the RX-DSP as introduced in this work.

application of a post-equalization (PE)-only where now the receiver bandwidth limits the resulting performance. Hence, to overcome spectral broadening introduced by Kerr-nonlinearity, one has to take into account an artificial bandwidth expansion. This required expansion combined with the LPF explains the performance drop of the split DBP at high launch powers.

The curves of Fig. 2 confirms the statement above. In green it shows the SE of the split DBP without the aforementioned LPFs. Indeed, it achieves the expected near optimal performance up to a certain launch power, where the drop can be related to, either, the limited accuracy of the SSFM, i.e., the number of steps N_{SSFM} used for the channel and the DBP, or, signal-noise-interaction. To get a better understanding of the accuracy, this system is evaluated at different number of SSFM steps. Enabling the LPFs one obtains the blue curve exhibiting a drop at lower launch powers than before. The space in between green and blue curve depicts the loss introduced only by spectral broadening.

For comparison (i) an upper bound proposed by Kramer et al. [19] that is equivalent to the Shannon limit and (ii) the constellation constrained MI I_{CC} for an additive white Gaussian noise (AWGN) channel based on hard decisions and assuming a 256-QAM are shown. The latter curve only indicates that, for low input powers, the conventional system achieves an almost optimal equalization. For high input powers, I_{CC} saturates as expected due to the constrained constellation.

2.3. Discussion of Conventional Reference Curves

Even if the DBP currently shows the best performance, and indeed compensates for the nonlinear impairments almost perfectly, this only holds for the case where, either, spectral broadening is not relevant, or, DAC, and/or ADC support a larger bandwidth than required by the actual information, at the expense of a higher TBP and, hence, lower SE by design. This gives rise to the assumption that better solutions than DBP in terms of SE exist for the case where both converters significantly limit the bandwidth. I.e., the goal is to enter the attainable region between the curves with and without LPF, indicated in yellow in Fig. 2. While this goal has not changed since [1], we now can apply both an extended AE and a new training procedure to further close this gap.

3. Autoencoder-optimized pulse shaping

Fig. 3 shows the block diagram of the new architectural template for the AE consisting of the TX in Fig. 3a and RX in Fig. 3b, where now both are trainable and nonlinear.

3.1. Brief recap of neural network notation

A network consists of an ordered set of layers $\mathcal{L} = \{L_1, L_2, \dots, L_\Theta\}$, where L_ϑ is the ϑ th layer of the total number of Θ layers. Here, a layer is

$$L_\vartheta : \mathbb{R}^{K_{\vartheta-1} \times D_{\vartheta-1}} \rightarrow \mathbb{R}^{K_\vartheta \times D_\vartheta} \quad (8)$$

$$\mathbf{U}_{\vartheta-1} \mapsto \mathbf{U}_\vartheta$$

where $\mathbf{U}_{\vartheta-1}$ is the input and \mathbf{U}_ϑ is the output signal of the ϑ th layer; $K_\vartheta \in \mathbb{N}$ is the length of the signal in terms of time samples after the ϑ th layer; and D_ϑ is the dimensionality of each time sample, i.e., the number of channel components. An example of channel components are real and imaginary part of a signal with $D_\vartheta = 2$. In the following $u_{\vartheta,k,d} = [\mathbf{U}_\vartheta]_{k,d}$ is element of a signal matrix at time instance k and component d . In this work a layer is either a convolutional or a dense layer, where $\vartheta = 0$ denotes the input signal.

For a convolutional layer $L_\vartheta = L_{\vartheta,\text{conv}}$, the output dimension D_ϑ corresponds to the number of different trainable kernels or filters $\mathbf{H}_{\vartheta,d} \in \mathbb{R}^{N_\vartheta \times D_{\vartheta-1}}$ for $d = 0, \dots, D_\vartheta - 1$; $N_\vartheta < K_\vartheta$ is the filter's individual length. All filters of a single layer have the same length. The output sample of a convolutional layer ϑ at time instance k and for output component d can be formulated as

$$u_{\vartheta,k,d} = L_{\vartheta,\text{conv}}(\mathbf{U}_{\vartheta-1}) = \varphi_\vartheta \left\{ \text{tr} \left(\bar{\mathbf{U}}_{\vartheta-1,k} \cdot \mathbf{H}_{\vartheta,d}^T \right) + b_{\vartheta,d} \right\} \quad (9)$$

where φ_ϑ is the activation function, $(\cdot)^T$ is the transpose, $b_{\vartheta,d}$ is a trainable bias, and

$$\bar{\mathbf{U}}_{\vartheta-1,k} = \begin{pmatrix} u_{\vartheta-1,k-\bar{N},0} & \cdots & u_{\vartheta-1,k-\bar{N},D_{\vartheta-1}-1} \\ \vdots & \ddots & \vdots \\ u_{\vartheta-1,k+\bar{N},0} & \cdots & u_{\vartheta-1,k+\bar{N},D_{\vartheta-1}-1} \end{pmatrix} \quad (10)$$

is a sliced and shifted version of the input signal with $\bar{N} = (N_\vartheta - 1)/2$. The filter length N_ϑ is always chosen

to be odd, to have a symmetric influence of the neighboring samples. A zero padding is added such that one obtains equal length of the input and output signal what is often referred to as “same” padding. This corresponds to $u_{\vartheta,k,d} = 0 \forall k < 0$ or $k \geq K_{\vartheta}$.

For a dense layer $L_{\vartheta} = L_{\vartheta,\text{dense}}$, the output dimension D_{ϑ} corresponds to the number of neurons of that layer and $N_{\vartheta} = 1 \forall \vartheta$ as, here, each layer operates on a single time instance k . This simplifies Eq. (9) to

$$\begin{aligned} u_{\vartheta,k,d} &= L_{\vartheta,\text{dense}}(\mathbf{U}_{\vartheta-1}) \\ &= \varphi_{\vartheta} \{ [\mathbf{U}_{\vartheta-1}]_k \cdot \mathbf{H}_{\vartheta,d}^T + b_{\vartheta,d} \}. \end{aligned} \quad (11)$$

3.2. Transmitter Design

Equivalent to the reference system, the symbol indices $\mathbf{s} \in \mathcal{M}^{N_B}$ shall be transmitted by the TX and estimated by the RX with a symbol rate of $R_s = 20$ GBd. Here, the same system parameters hold as already given in Sec. 2. Each transmission contains a batch of $N_B = 12,000$ symbol indices, which is chosen on the basis of available GPU-memory in our simulation setup.

The TX as given in Fig. 3a starts with a trainable mapping, i.e., an $M \times 2$ -matrix, choosing symbols \mathbf{c} from a complex constellation based on the incoming symbol indices \mathbf{s} . Then, the signal is upsampled from symbol rate R_s to $u_{\text{sam}} \cdot R_s$ by adding zeroes in between the in-phase quadrature (IQ)-symbols, and, subsequently, pulse shaped. Here, $u_{\text{sam}} = 4$ has shown to be sufficiently large to achieve the results in the following figures, staying well below the upsampling of the DBP, where $u_{\text{sam}} = 50$.

The nonlinear pulse shaping generates the waveform \mathbf{x}_{CNN} and is realized by a convolutional neural network (CNN). As such, it can only process real valued signals, and, thus, the two transformations $\mathbb{C}2\mathbb{R}^2$ and $\mathbb{R}^22\mathbb{C}$ vice-versa are required. Thereby, real and imaginary part of the complex signal are stacked in an additional last dimension.

It follows an upsampling from sample rate $u_{\text{sam}} \cdot R_s = 80$ GHz of the CNN to $f_{\text{sim}} = 1$ THz, now including a Whittaker-Shannon interpolation for quasi-continuous waveform channel simulation. The lowpass-filtered and power normalized signal \mathbf{x} is finally transmitted over

TABLE 2: Parameters of the TX- and RX-NN.

Layer	Type	Parameters		
		D_{ϑ}	N_{ϑ}	φ_{ϑ}
Transmitter				
1	Convolutional	128	221	linear
2	Dense	64	-	elu
3	Dense	64	-	elu
4	Dense	64	-	elu
5	Dense	2	-	linear
Receiver				
1	Convolutional	128	55	linear
2	Dense	2048	-	elu
3	Dense	2048	-	elu
4	Dense	512	-	elu
5	Dense	512	-	elu
6	Dense	512	-	elu
7	Dense	256	-	linear

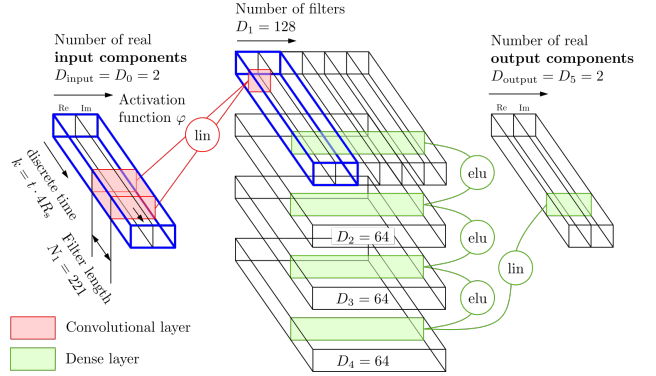


Figure 4: CNN used at TX. Boxes depict the signals \mathbf{U}_{ϑ} . Bold blue lines depict the equivalent (linear) structure of [1] with $D_{\text{output}} = D_1 = 2$.

the channel, with samples being calculated as $[\mathbf{x}]_k = g_{\text{TX}}(k, \mathbf{s}; \Omega_{\text{TX}})$. Here, g_{TX} summarizes the TX function with trainable parameters Ω_{TX} , i.e., the weights \mathbf{H}_{ϑ} .

The design of the TX CNN of Fig. 3a is shown in Fig. 4, with the parameters given in Tab. 2. It is motivated by the fact that neighboring symbols nonlinearly interact with each other along the fiber. The input signal of the CNN is $\mathbf{U}_0 = \mathbf{C}_{\text{Re}} \in \mathbb{R}^{u_{\text{sam}} N_B \times 2}$. Hence, the input length $K_0 = u_{\text{sam}} N_B$ is the sequence of constellation symbols upsampled by u_{sam} . The input dimension $D_0 = 2$ represents real and imaginary part of the original complex signal. The first layer is a convolutional layer that convolves its $D_1 = 128$ different filter kernels $\mathbf{H}_{1,d} \in \mathbb{R}^{N_1 \times D_0}$ for $d < D_1$ with the real and imaginary part of the input signal. The length

$$N_1 = \lceil \Delta t_{\text{CD}} \cdot R_s \rceil \cdot u_{\text{sam}} + 1 = 221 \quad (12)$$

is chosen such that the filter length is in the order of the pulse widening induced by chromatic dispersion (CD) of

$$\Delta t_{\text{CD}} = 2\pi\beta_2 \ell B_w. \quad (13)$$

Also the dimension D_1 is derived from the pulse widening such that this layer is *at least* able to shift all relevant neighboring symbols to the same time instance by a (probably learned) time shifting filter $\mathbf{H}_{\text{shift}} = (\delta_{-D_1,k}, \dots, \delta_{D_1,k})$ with Kronecker-Delta

$$\delta_{n,k} = \begin{cases} 1 & k = n \\ 0 & \text{else} \end{cases} \quad (14)$$

and $k \in \{0, \dots, K_1 - 1\}$. Hence, we have chosen $D_1 = 128 \gg \lceil \Delta t_{\text{CD}} \cdot R_s \rceil = 55$. It follows a sub-network consisting of dense layers that operate on the single time instances of the D_1 convolved signals. The last layer again produces $D_5 = D_0 = 2$ time signals that form the real and imaginary part of the pre-distorted signal $\mathbf{x}_{\text{CNN}} = \mathbb{R}^22\mathbb{C}\{\mathbf{U}_5\}$.

Bold blue lines mark the TX-structure of the former AE applied in [1]. Hence, the case $D_1 = 2$ and an imposed constraint on the kernel to perform a complex convolution, corresponds to the earlier TX, i.e., the former structure is a special case of the one provided here, respectively.

3.3. Receiver Design

The computational efficiency of the overlap & save mechanism from [1] was not sufficient to be exhaustively trained such that we have had to deviate more from this intuitive design to reduce complexity. Hence, what follows is a CNN that substitutes the overlap & save mechanism in a more efficient way while having at least the same degree of freedom. Nevertheless, the achieved gains of the new architecture stem from the TX.

The RX as shown in Fig. 3b consists of blocks for downsampling the receive signal \mathbf{y} from simulation frequency f_{sim} to symbol rate R_s , a complex-to-real-transformation, and a CNN to learn an estimate of the desired likelihoods $\hat{l}_{k,m} = \hat{P}(S_k = m|\mathbf{y})$ of the transmitted symbol indices S_k based on the received signal \mathbf{y} . Note that S_k denotes the random variable (RV) corresponding to the true transmitted symbol index s_k at time instance k and a realization $m \in \mathcal{M}$. This can be obtained by a row-wise softmax-normalization of the CNN's output $[\mathbf{L}]_{k,m} = \hat{l}_{k,m}$ and appropriate cost function as described below. The whole block can be written as a trainable function such that $\hat{l}_{k,m} = g_{\text{RX}}(k, m, \mathbf{y}; \Omega_{\text{RX}})$ with parameters Ω_{RX} that consists of the weights \mathbf{H}_θ of the RX-NN. In a last step, the symbol with highest likelihood is chosen to be the hard decided estimate

$$\hat{s}_k = \arg \max_m g_{\text{RX}}(k, m, \mathbf{y}; \Omega_{\text{RX}}) \in \mathcal{M}. \quad (15)$$

The CNN has the same architecture as in Fig. 3 but with different parameters, given in Tab. 2. The number of output neurons of the last layer is M and has a linear activation function. The softmax-normalized output, then, can be interpreted as the previously introduced likelihoods of the transmit symbol.

4. Training using γ -Lifting

The general objective of the trainable AE is an optimal estimate of the transmitted symbols at RX

$$\hat{\mathbf{s}} \stackrel{\dagger}{=} \mathbf{s} \Rightarrow \hat{s}_k \stackrel{\dagger}{=} s_k \forall k, \quad (16)$$

where \mathbf{s} is the vector containing the transmitted symbol indices, and $\hat{\mathbf{s}}$ the corresponding estimate by the RX.

To achieve this goal, the parameters $\Omega = \{\Omega_{\text{TX}}, \Omega_{\text{RX}}\}$ of TX and RX are trainable, which is common for all AE-setups in communications. Hence, not only TX and RX, but the whole AE system of Fig. 1a can be seen as a trainable function $g(k, m, \mathbf{s}; \Omega)$. This way, the estimate of the symbol at time instance k is the argument of the maximization of the learned probabilities over all symbol indices $\hat{s}_k = \arg \max_m g(k, m, \mathbf{s}; \Omega)$ with $m \in \mathcal{M}$. Having said this, the objective can be further detailed to $g(k, m, \mathbf{s}; \Omega) = \hat{P}(S_k = m) \stackrel{\dagger}{=} P(S_k = m) \forall k$, where

$$P(S_k = m) = \begin{cases} 1, & m = s_k \\ 0, & \text{else} \end{cases} \quad (17)$$

is the probability mass function (PMF) of the true transmit symbol indices $s_k = [\mathbf{s}]_k$ (this refers to ‘‘one-hot encoding’’, as the PMF of the transmitted symbols corresponds to the Kronecker-delta). The optical channel is contained

in $g(k, m, \mathbf{s}; \Omega)$ and serves as the penalty to overcome by choosing Ω appropriately.

Equivalent to [1], we trained the AE using samplewise cross-entropy (CE) loss for batch sample k defined as

$$\begin{aligned} \mathcal{L}_{\text{CE}} \left(P(S_k = m), \hat{P}(S_k = m) \right) \\ = \mathbb{H}_{P(S_k = m)} \left[\hat{P}(S_k = m) \right] \end{aligned} \quad (18)$$

where $\mathbb{H}[\cdot]$ is cross-entropy and $\mathbb{E}[\cdot]$ is expectation. Taking into account Eq. (17) this can be further simplified to

$$\mathcal{L}_{\text{CE}} \left(P, \hat{P} \right) = -\log g(k, m = s_k, \mathbf{s}; \Omega) \quad (19)$$

The resulting cost is defined over the batch of symbols with size N_B and calculates as

$$\begin{aligned} \mathcal{C}_{\text{CE}} \left(P(S_k = m), \hat{P}(S_k = m) \right) \\ = -\frac{1}{N_B} \sum_{k=0}^{N_B-1} \log g(k, m = s_k, \mathbf{s}; \Omega) \end{aligned} \quad (20)$$

For the optimizer we have chosen Adam [22], which applies stochastic gradient descent (SGD) to minimize the cost as

$$\Omega_{\text{opt}} = \arg \min_{\Omega} \mathcal{C}_{\text{CE}} \left(P, \hat{P} \right) \quad (21)$$

by training the parameters Ω . For a conventional training as in [1] the channel is fixed and only training parameters, i.e., the learning rate w_{lr} and batch size N_B , are adjusted during training to support convergence. The latter is achieved by the aid of the training configuration of Tab. 3.

Nevertheless, the very first results have shown that the training procedure of [1] is not sufficient to train the proposed architectural template. Only by repeating the training given in Tab. 3, by chance, we obtain the dashed red results of Fig. 5b. The underlying problem is depicted also in dashed red in Fig. 5a, where one can see that the performance jumps during the first training cycles, i.e., repetitions. Having realized that convergence is a major problem of training the AE through the SSFM, we further investigated on how to increase the stability of the convergence and to probably find better local optima. Hence, in the following we introduce a new training method that was inspired by the training described in [23]. There, the input training samples were chosen such that the learning gets simplified or, i.e., the relation between input and output becomes more obvious to the trainable structure.

We have searched for a way to simplify the stated problem such that we can gradually converge until finally arriving at the desired more complex problem to solve.

TABLE 3: Configuration of a single training cycle.

Max. training iterations	Batch size	Learning rate
N_{train}	N_B	w_{lr}
2000	12,000	$2 \cdot 10^{-4}$
1500	12,000	$1 \cdot 10^{-4}$
1000	12,000	$5 \cdot 10^{-5}$
500	12,000	$1 \cdot 10^{-5}$

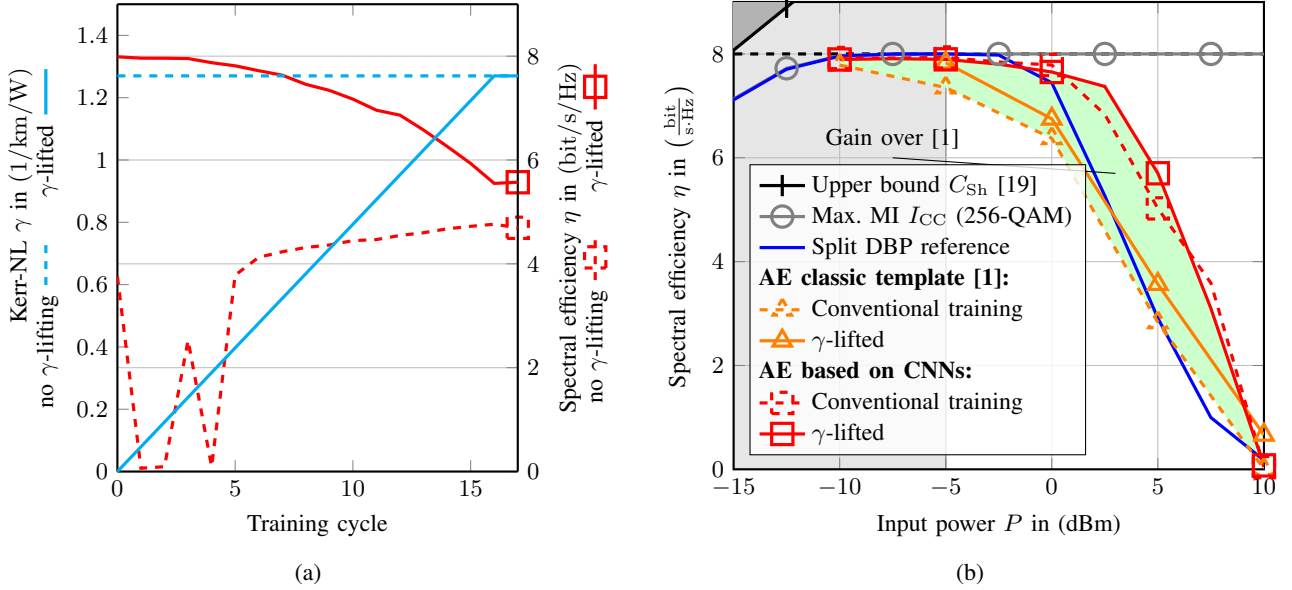


Figure 5: Performance evaluation of the AE based on CNN with (a) showing the γ -lifting that describes the increase of γ over training cycle on the left axis and the resulting SE on the right axis at $P = 5$ dBm; and (b) over input power compared to the different AEs with γ -lifting (solid) and without (dashed).

Here, this may be achieved by setting some channel parameters to zero and increasing them incrementally, which, in effect, results in an *increasing difficulty* for training the system. Thereby, we ensure that training converges in each cycle, before making it harder. As potential parameters we identified the following:

Slowly increasing fiber length ℓ simplifies the problem significantly as all impairments increase with fiber length. On the downside, it poses an unsolvable conflict between a varying accuracy and a vanishing gradient information. This can be seen by considering the step size of the SSFM $\Delta z_{SSFM} = \ell / N_{SSFM}$. A growing ℓ means either an increasing Δz_{SSFM} and hence a varying accuracy; or adaption of N_{SSFM} , which means that the error has to be backpropagated through an increasing number of SSFM-iterations. This way, the very first training cycles may be predominant compared to the later ones with weaker gradient information. Using chromatic dispersion β_2 means reducing inter-symbol interference (ISI) at the beginning and incrementally adding more influence of neighboring symbols. This allows to start with a simple sample-wise compensation at the beginning, but is in contrast to the requirement that the filter length N_θ of the CNN has to be fixed to the final length over all trainings, anyway. Hence, for the first training cycles, most of the randomly initialized trainable filter taps rather distort than may ever support. For considering Kerr-effect only, γ controls the power-dependent rotation of a sample, where, in turn, its power depends on the corresponding transmit symbol, neighboring transmit symbols, and noise. Reducing γ disentangles the simple linear superposition of CD and may help to learn their interactions step-by-step.

As there is no obvious drawback connected to the Kerr-nonlinearity parameter, we decided to use a γ -lifting. This γ -over-cycle dependency is also depicted in Fig. 5a for $P = 5$ dBm by the solid cyan curve, which linearly increases with training cycle. Note that, each training

cycle consists of all training iterations described by Tab. 3. The conventional training is depicted by the dashed cyan curve showing that γ is constant. It may be misleading that the SE worsens over training cycle, which is a consequence of the increasing difficulty. Nevertheless, comparing both red curves – the one without γ -lifting (dashed) and the one with (solid) – shows that the latter exhibits a significantly stabilized convergence, as no large variations can be observed anymore. Further, it achieved a significantly higher SE for the final $\gamma = 1.27 \text{ km}^{-1} \text{ W}^{-1}$, i.e., 5.7 bit/s/Hz vs. 5.0 bit/s/Hz.

Performing γ -lifting over the whole input power space results in Fig. 5b. The dashed curves again show the earlier AE (orange) and the one proposed in this work (red) with their conventional training. Switching on γ -lifting leads to the corresponding solid curves. It can be seen that γ -lifting, in most cases, pushes the performance of the CNN-based AE closer to I_{CC} . By chance, thereby, the conventional training may still exceed the γ -lifting due to the high fluctuations in the training quality. Nevertheless, the proposed AE outperforms the former AE as well as the split DBP at high input powers. This means that we have compensated or avoided spectral broadening partly and may operate at higher launch powers, which may be beneficial for higher modulation formats or reach. Even by the application of γ -lifting to this former AE, its performance stays well below the one proposed here, due to the limitations of its linear architectural template. The CNN-based AE is not able to reach the numerical limit that was introduced by Fig. 2, but significantly contributes to closing this gap.

5. Summary and conclusion

In this work, we have identified spectral broadening introduced by Kerr-nonlinearity as one of the major per-

formance limitation of a DBP for the simulated optical fiber channel with bandlimited TX and RX.

The nowadays well-known AE was chosen as an approach to learn to address this challenge and to find an appropriate nonlinear pulseshaping. We showed that the TX-part of the AE can be trained through the SSFM. As it turned out, a stable convergence of the trainable structures requires a carefully adjusted training method. We have therefore combined a conventional training with a novel “ γ -lifting” strategy to achieve significant gains compared to the currently best known NLC schema, i.e., split DBP, in a regime where spectral broadening is significant.

For now, we have only considered a single channel and single polarization scenario, to obtain a better understanding of the effects of Kerr-nonlinearity. In future work, these ideas can be extended to a multi-channel system (wavelength division multiplex (WDM)), or by applying even more sophisticated architectural templates.

References

- [1] T. Uhlemann, S. Cammerer, A. Span, S. Dörner, and S. ten Brink, “Deep-learning Autoencoder for Coherent and Nonlinear Optical Communication,” in *Photonic Networks; 21st ITG-Symposium*, 2020.
- [2] D. S. Millar, S. Makovejs, C. Behrens, S. Hellerbrand, R. I. Killey, P. Bayvel, and S. J. Savory, “Mitigation of Fiber Nonlinearity Using a Digital Coherent Receiver,” *IEEE Journal of Selected Topics in Quantum Electronics*, vol. 16, no. 5, pp. 1217–1226, Sep. 2010.
- [3] M. I. Yousefi and F. R. Kschischang, “On the Per-Sample Capacity of Nondispersive Optical Fibers,” *IEEE Transactions on Information Theory*, vol. 57, no. 11, pp. 7522–7541, 2011.
- [4] T. Xu, B. Karanov, N. A. Shevchenko, D. Lavery, G. Liga, R. I. Killey, and P. Bayvel, “Digital nonlinearity compensation in high-capacity optical communication systems considering signal spectral broadening effect,” *Scientific Reports*, vol. 7, no. 1, p. 12986, Dec. 2017.
- [5] R.-J. Essiambre, G. Raybon, and B. Mikkelsen, “Chapter 6 - Pseudo-Linear Transmission of High-Speed TDM Signals: 40 and 160 Gb/s,” in *Optical Fiber Telecommunications IV-B (Fourth Edition)*, fourth edition ed., ser. Optics and Photonics, I. P. Kaminow and T. Li, Eds. Burlington: Academic Press, 2002, pp. 232–304.
- [6] D. M. Pepper and A. Yariv, “Compensation for phase distortions in nonlinear media by phase conjugation,” *Optics Letters*, vol. 5, no. 2, p. 59, Feb. 1980.
- [7] E. Bidaki and S. Kumar, “A Raman-Pumped Dispersion and Nonlinearity Compensating Fiber For Fiber Optic Communications,” *IEEE Photonics Journal*, vol. 12, no. 1, pp. 1–17, Feb. 2020.
- [8] K. Peddanarappagari and M. Brandt-Pearce, “Volterra series transfer function of single-mode fibers,” *Journal of Lightwave Technology*, vol. 15, no. 12, pp. 2232–2241, Dec. 1997.
- [9] X. Li, X. Chen, G. Goldfarb, E. Mateo, I. Kim, F. Yaman, and G. Li, “Electronic post-compensation of WDM transmission impairments using coherent detection and digital signal processing,” *Optics Express*, vol. 16, no. 2, p. 880, 2008.
- [10] A. Mecozzi and R.-J. Essiambre, “Nonlinear Shannon Limit in Pseudolinear Coherent Systems,” *Journal of Lightwave Technology*, vol. 30, no. 12, pp. 2011–2024, Jun. 2012.
- [11] M. I. Yousefi and F. R. Kschischang, “Information Transmission Using the Nonlinear Fourier Transform, Part III: Spectrum Modulation,” *IEEE Transactions on Information Theory*, vol. 60, no. 7, pp. 4346–4369, Jul. 2014.
- [12] B. Karanov, M. Chagnon, F. Thouin, T. A. Eriksson, H. Bulow, D. Lavery, P. Bayvel, and L. Schmalen, “End-to-End Deep Learning of Optical Fiber Communications,” *Journal of Lightwave Technology*, vol. 36, no. 20, pp. 4843–4855, Oct. 2018.
- [13] D. Lavery, D. Ives, G. Liga, A. Alvarado, S. J. Savory, and P. Bayvel, “The Benefit of Split Nonlinearity Compensation for Single-Channel Optical Fiber Communications,” *IEEE Photonics Technology Letters*, vol. 28, no. 17, pp. 1803–1806, Sep. 2016.
- [14] C. Häger and H. D. Pfister, “Physics-Based Deep Learning for Fiber-Optic Communication Systems,” *IEEE Journal on Selected Areas in Communications*, vol. 39, no. 1, pp. 280–294, 2021.
- [15] V. Neskorniuk, A. Carnio, V. Bajaj, D. Marsella, S. K. Turitsyn, J. E. Prilepsky, and V. Aref, “End-to-End Deep Learning of Long-Haul Coherent Optical Fiber Communications via Regular Perturbation Model,” in *2021 European Conference on Optical Communication (ECOC)*, 2021, pp. 1–4.
- [16] A. Span, V. Aref, H. Bulow, and S. ten Brink, “Time-Bandwidth Product Perspective for Nonlinear Fourier Transform-Based Multi-Eigenvalue Soliton Transmission,” *IEEE Transactions on Communications*, vol. 67, no. 8, pp. 5544–5557, Aug. 2019.
- [17] S. Gaiarin, F. Da Ros, R. T. Jones, and D. Zibar, “End-to-End Optimization of Coherent Optical Communications Over the Split-Step Fourier Method Guided by the Nonlinear Fourier Transform Theory,” *Journal of Lightwave Technology*, vol. 39, no. 2, pp. 418–428, Jan. 2021.
- [18] G. P. Agrawal, *Nonlinear fiber optics*. Springer, 2000.
- [19] G. Kramer, M. I. Yousefi, and F. R. Kschischang, “Upper bound on the capacity of a cascade of nonlinear and noisy channels,” in *2015 IEEE Information Theory Workshop (ITW)*. Jerusalem, Israel: IEEE, Apr. 2015, pp. 1–4.
- [20] R.-J. Essiambre, G. Kramer, P. J. Winzer, G. J. Foschini, and B. Goebel, “Capacity Limits of Optical Fiber Networks,” *Journal of Lightwave Technology*, vol. 28, no. 4, pp. 662–701, Feb. 2010.
- [21] K. Roberts, Chuandong Li, L. Strawczynski, M. O’Sullivan, and I. Hardcastle, “Electronic precompensation of optical nonlinearity,” *IEEE Photonics Technology Letters*, vol. 18, no. 2, pp. 403–405, Jan. 2006.
- [22] D. P. Kingma and J. Ba, “Adam: A Method for Stochastic Optimization,” *arXiv:1412.6980 [cs]*, Jan. 2017, arXiv: 1412.6980.
- [23] D. Tandler, S. Dörner, S. Cammerer, and S. ten Brink, “On Recurrent Neural Networks for Sequence-based Processing in Communications,” in *2019 53rd Asilomar Conference on Signals, Systems, and Computers*. Pacific Grove, CA, USA: IEEE, Nov. 2019, pp. 537–543.